Efficient screening of materials and fast optimization of vapor deposited OLED characteristics

Christoph Schmitz, Peter Pösch, Mukundan Thelakkat and Hans-Werner Schmidt*

Makromolekulare Chemie I, Universität Bayreuth and Bayreuther Institut für Makromolekülforschung (BIMF), D-95440 Bayreuth, Germany

SUMMARY: A combinatorial approach combining vapor deposition of organic molecules and a movable mask technique was used to screen and optimize materials and organic light emitting device configurations fast and efficiently. Some low molecular weight triphenyldiamine derivatives with different electronic and thermal properties were compared in two layer, ITO/TPD/Alq_3/Al device configurations. The optimum thickness for Alq_3 layer was obtained by evaporating a linear gradient of Alq_3 on top of various TPD layers. Further, a landscape library with two orthogonal linear gradients of TPD and Alq_3 was prepared to investigate the dependence of efficiency on thickness of both layers simultaneously. The necessity and the efficiency of an additional spiro-qunioxaline compound as electron transporting/hole blocking layer was also investigated using a landscape library of Alq_3 versus spiro-quinoxaline on top of TPD. The efficiency of the two layer device depends not only on the Alq_3 layer thickness, but also on the TPD layer thickness. The photometric efficiency of a TPD/Alq_3 device can be improved by replacing the optimum Alq_3 layer thickness by certain combinations of Alq_3/spiro-quinoxaline layers.

Introduction

Organic electroluminenscent displays are one of the realized emerging flat panel display concepts of the next century[1,2]. The thin layer organic light emitting devices (OLEDs) fabricated by vacuum deposition technology, first demonstrated by Tang et al. in 1987[3], are meanwhile commercialized as low information content displays [4,5]. In the current stage of the development of this technology, it is important to carry out a fast screening and optimization of different materials and device configurations with respect to materials properties, layer thicknesses, deposition parameters and layer composition under comparable and reproducible conditions. It is very tedious and time-consuming if these parameters are optimized in a conventional way, by varying only one parameter at a time. To overcome this drawback we utilized a combinatorial concept to build up libraries of different OLEDs in order to screen and optimize device parameters[6,7]. Hanak et al. have already applied a similar approach in the

 CCC 1022-1360/00/$ 17.50+.50/0

preparation and analysis of inorganic solar cells and inorganic electroluminescent (EL) systems[8,9]. The combinatorial method presented here enables the optimization of OLEDs substantially faster by varying the parameters simultaneously than conventional one by one preparation.

In this contribution, the combinatorial approach was used to optimize the Alq_3-layer thickness on top of different HTLs with constant thickness as well as to examine the dependence of device efficiency on both TPD and Alq_3 layer thicknesses[7]. Further, the effect of an additional electron transport layer (ETL) in enhancing the device performance was investigated[6]. The most widely applied materials for electron transport are π-electron deficient heterocyclics with aromatic nitrogen atoms, such as 1,3,4-oxadiazoles, 1,2,4-triazoles, 1,3,5-triazines or 1,4-quinoxalines. These materials are considered to support electron injection, electron transport and function additionally as hole blocking material[7]. A low molecular weight compound, spiro-quinoxaline, was applied as ETL on top of a two layer device.

Experimental

Materials:

N,N´-Bis-(4-methoxyphenyl)-N,N´-diphenylbenzidine (TPD 1), N,N´-bis(4-phenoxyphenyl)-N,N´-diphenylbenzidine (TPD 2) and N,N´-bis(4-phenanthryl)-N,N´-diphenylbenzidine (TPD 3) were synthesized according to a known procedure[10]. The synthesis of spiro-quinoxaline is given elsewhere[6]. Alq_3 was purchased from Aldrich and used without any further purification.

Combinatorial set-up and device preparation:

An apparatus consisting of a movable mask sledge and a rotatable substrate holder was developed to be used in a vacuum deposition chamber. By positioning suitable masks and by rotation of the substrate holder, sectors with different material composition were created on one single substrate. By gradual movement of the mask combined with substrate rotation, orthogonal linear gradients of film thicknesses can be deposited. The dimensions of the substrate used was 7.6 cm x 7.6 cm with an area of 57.76 cm^2. Aluminum was deposited as a final step either as stripes (1.77x18 mm) or as dots (d = 4,9 mm).

Instrumentation:

Current-voltage characteristics were measured using a computerized set up consisting of a luminometer LS 100 by Minolta, a multimeter Keithley 2000 and a programmable power supply PN 300 by Grundig. The layer thicknesses were determined with a surface profilometer (Dektak 3030 ST). The thermal characterization was performed on a DSC 7 (Perkin Elmer). Cyclic voltammetry measurements were carried out using a three electrode cell and potentiostat assembly from EG&G Princeton Applied Research.

Results and discussion

The hole transport materials used in this study are derivatives of triphenyldiamines (TPDs). The chemical structures of the TPDs and spiro-quinoxaline (spiro-Qux) are given in fig. 1.

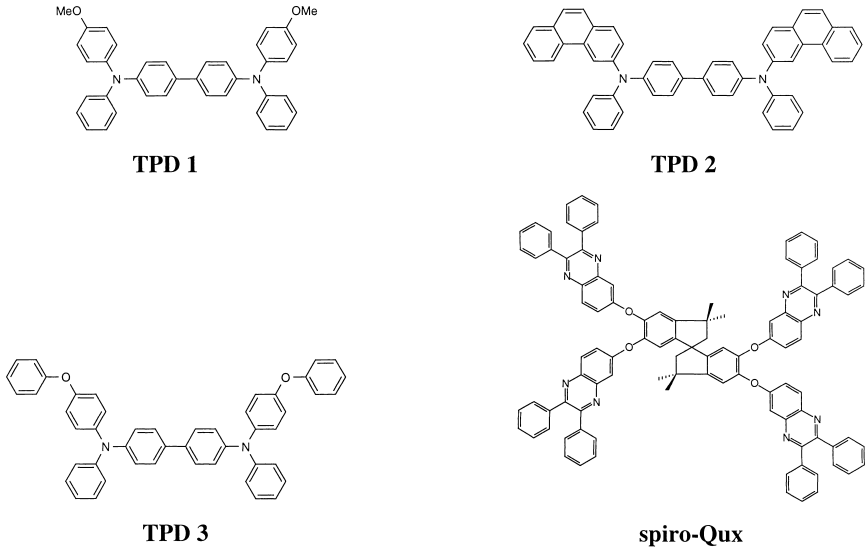

Fig. 1: Chemical structures of N,N´-bis(4-methoxyphenyl)-N,N´-diphenylbenzidine (TPD 1), N,N´-bis(4-phenoxyphenyl)-N,N´-diphenylbenzidine (TPD 2), N,N´-bis(4-phenanthryl)-N,N´-diphenylbenzidine (TPD 3) and spiro-quinoxaline (spiro-Qux).

All the three TPD derivatives show a melting peak in the first heating cycle only. No recrystallization was observed on cooling with 10 K/min from the melt or in the second heating run. Stable amorphous films were obtained by vapor deposition of TPD 1-3. The HOMO values of TPD 1-3 determined from the first oxidation potentials (from cyclic

voltammetry; CV) with respect to ferrocene/ferrocenium as internal standard are -5.06 eV, -5.12 eV and -5.17 eV, respectively. These values are in the typical range of similarly substituted TPD derivatives[11,12]. The glass transition temperature of spiro-Qux as determined from differential scanning calorimetry (DSC) is at 155 °C. The material forms stable amorphous film on vapor deposition. The LUMO energy value of spiro-Qux (from CV) is -2,79 eV. This low LUMO value favors the electron injection from an aluminum cathode.

In the first experiment two layer devices, ITO/HTL/Alq_3/Al, with different Alq_3 layer thicknesses on top of a constant layer thickness of TPD were prepared to investigate the influence of Alq_3 layer thickness on device characteristics. The ITO/glass substrates (dimension: 7.6 cm x 7.6 cm, area: 57.76 cm^2, ITO-thickness: 110 nm, sheet resistance: 30 Ω/□) were etched on both sides 10.0 mm wide to avoid shorts between ITO and aluminum during contacting. The different steps of device preparation are illustrated in fig. 2.

1. Step: Vapor deposition of TPDs with constant thickness

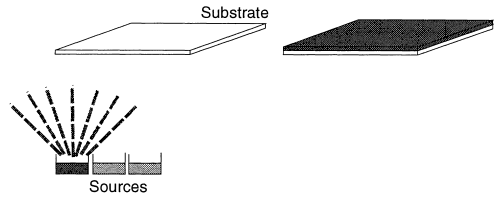

2. Step: Vapor deposition of linear gradient of Alq_3

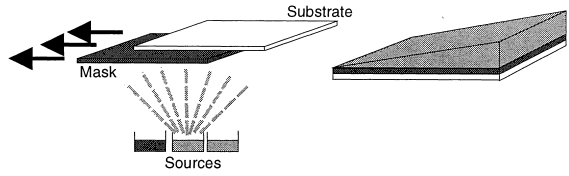

3. Step: Vapor deposition of aluminum through a mask

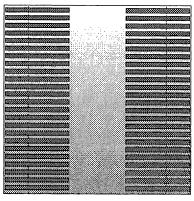

Fig. 2: Device preparation steps for the optimization of Alq_3 layer thickness on top of a hole transport layer with constant thickness.

In step 1, the low molecular weight TPDs were vapor deposited on top of an ITO/glass substrate to obtain a constant layer thickness. The layer thicknesses for the different TPDs are TPD 1 (70 nm), TPD 2 (60 nm) and TPD 3 (50 nm), respectively. As second step, a linear gradient of Alq_3 (0 - 150 nm) was vapor deposited over the whole substrate on top of the TPD layer by continuous shutter movement. In a final step 200 nm thick aluminum stripes were vapor deposited as cathode through a mask with 24 stripes on both sides of the substrate. The active area of each device is 0.32 cm^2 (1.77 mm x 18 mm). There is a linear gradient of 3.5 nm Alq_3 within each OLED. The layer thicknesses were measured in the middle of each stripe. All vapor depositions were proceeded at a pressure of about 10^{-6} mbar. Using the described preparation steps, we obtained various devices with combinations of constant TPD layer thickness and different Alq_3 layer thicknesses in one experiment. This enables us to find the optimum Alq_3 layer thickness with respect to power efficiency, photometric efficiency and current-voltage characteristics very fast.

a) b)

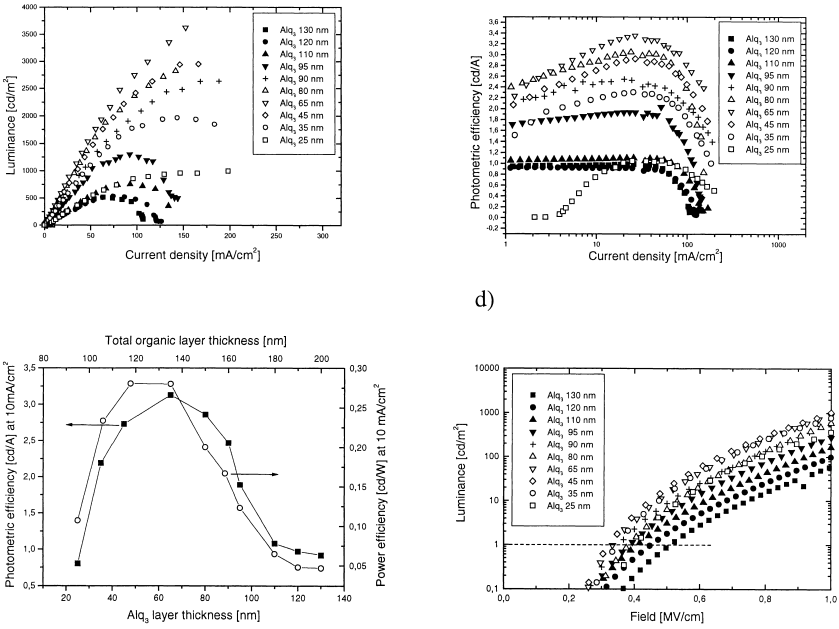

Fig. 3: Efficiency plots for the device: ITO/TPD 1 (70 nm)/Alq_3-gradient/Al:
a) luminance versus current density; b) photometric efficiency versus current density; c) photometric efficiency (-■-) and power efficiency (-O-) at 10mA/cm^2 versus Alq_3 and total organic layer thickness, d) luminance versus field.

As an example, the details of the device characteristics for the device, ITO/TPD 1 (70 nm)/Alq_3 (0-150nm)/Al are shown in fig. 3. The variation of luminance as a function of current density is plotted in fig. 3a. The device ITO/TPD 1 (70 nm)/Alq_3 (65 nm)/Al has the highest slope for the luminance versus current density plot. This device also shows the maximum luminance of about 3600 cd/m² at a current density of 150 mA/cm^2. With increasing or decreasing Alq_3 layer thickness from the optimum value of 65 nm, the efficiency and the luminance decrease. This is better illustrated in fig. 3b in which the photometric efficiency [cd/A] is plotted versus current density. The maximum efficiency of 3.4 cd/A is achieved for the device with an Alq_3 layer thickness of 65 nm. In fig. 3c the variation of both photometric efficiency and power efficiency (at 10 mA/cm^2) is plotted as a function of Alq_3 thickness and total organic layer thickness. The curves reveal the extreme dependence of both efficiencies on Alq_3 layer thickness. The maximum power efficiency of 0.28 cd/W is achieved for the device with an Alq_3 layer thickness of 45 nm. However the device with 65 nm thick Alq_3 layer has the maximum photometric efficiency. Fig. 3d depicts the variation of luminance with respect to applied field. In this way the dependence of onset voltage on Alq_3 layer thickness was examined. To obtain a luminance of 1 cd/m², the field can be decreased from 0.4 MV/cm (4 V) to 0.3 MV/cm (3.5 V) on increasing Alq_3 layer thickness from 25 nm to 45 nm. On further increasing Alq_3 thickness the onset increases from 0.3 MV/cm to 0.5 MV/cm (10 V). Thus the device ITO/TPD 1 (70 nm)/Alq_3 (45 nm)/Al has the lowest onset. This coincides with the observation of the maximum power efficiency for this particular device. The current flow in all the devices is proportional to the luminance. For a constant current density, the field increases continuously in devices with increasing Alq_3 thickness (plot not given). The existence of an optimum Alq_3 layer thickness for a constant layer thickness of HTL in such two layer devices is in agreement with the published results of Forrest et al.[13]. Compared to the time consuming one by one optimization the advantage of the presented method is the much faster device preparation in one single experiment. Thus, using the described combinatorial method we are able to determine different layer thickness combinations of TPD and Alq_3 suitable for the best photometric and power efficiency in a fast and efficient way.

In an analogous device structure, TPD 2 and TPD 3 were examined. The devices have the following configurations: ITO/TPD 2 (60 nm)/Alq_3 (0-150 nm)/Al and ITO/TPD 3 (50 nm)/Alq_3 (0-150 nm)/Al. Fig. 4 compares the Alq_3 thickness dependence of the photometric efficiency and power efficiency (at 10mA/cm^2) for the various HTL materials.

The existence of an optimum Alq_3 thickness and a considerable dependence of efficiency on Alq_3 thickness is observed in all these devices.

a) b)

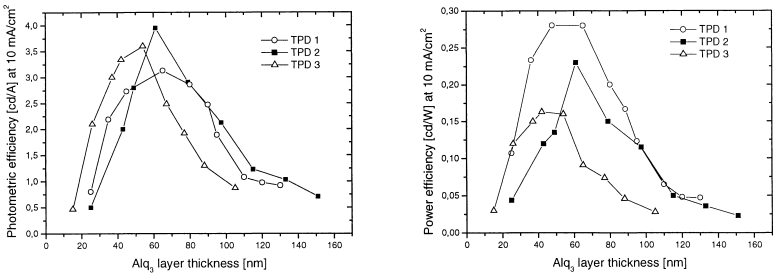

Fig. 4: a) photometric efficiency and b) power efficiency plotted for the different TPDs 1-3 as a function of Alq_3 layer thickness: -O- TPD 1 (70 nm), -■- TPD 2 (60 nm) and -Δ- TPD 3 (50 nm).

In order to examine the influence of HTL thickness on efficiency, a landscape library for the variation of both TPD 1 and Alq_3 layer thickness was produced[7]. For device preparation, first a linear gradient of TPD 1 (0-100 nm) was vapor deposited on the ITO substrate followed by a 90° rotation of the substrate and subsequent vapor deposition of Alq_3 as an orthogonal linear gradient (0-150 nm). As a final step aluminum was deposited as 49 dots (7 columns x 7 rows) through a mask with an active area of 0.19 cm^2 (radius: 2.45 mm). The thickness of TPD 1 varies along the rows and the thickness of Alq_3 varies along the columns. In this way it was possible to prepare OLEDs with different combinations of TPD 1 and Alq_3 layer thicknesses. It is not at all possible to carry out such a landscape library for the variation of two parameters simultaneously in a conventional way maintaining the other parameters constant. In horizontal rows one to seven, the TPD layer thicknesses are 11 nm, 24 nm, 37 nm, 50 nm, 62 nm, 75 nm and 87 nm, respectively (measured at the middle of each spot). In vertical columns 1 - 7, the Alq_3 layer thicknesses are 6 nm, 26 nm, 46 nm, 66 nm, 86 nm, 106 nm and 126 nm, respectively. In fig. 5a and 5b the photometric efficiency and the power efficiency (both at 10 mA/cm^2) of the devices for varying thickness of TPD and Alq_3 are shown as three dimensional plots.

It can be clearly seen that the efficiency of the OLEDs vary not only with Alq_3 thickness, but also with TPD 1 layer thickness. It should be emphasized that the dependence of photometric efficiency on the Alq_3 layer thickness is much greater than that on the variation of TPD 1 layer thickness.

a) b)

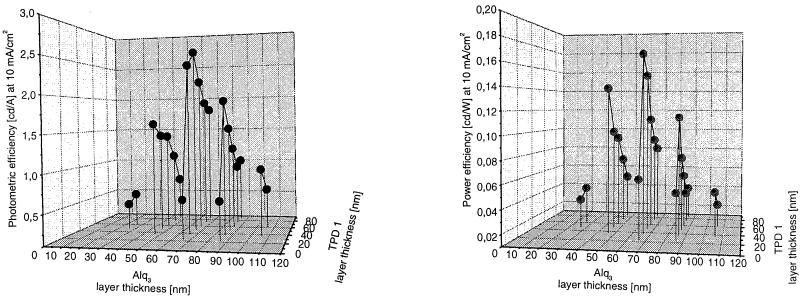

Fig. 5: a) Three dimensional plot of photometric efficiency and b) power efficiency versus Alq_3 and TPD 1 layer thicknesses.

On the other hand, the power efficiency depends almost to an equal extent on both TPD 1 and Alq_3 layer thicknesses. The different combinations of TPD 1 and Alq_3 layer thicknesses reveal the most efficient device as ITO/TPD 1 (50nm)/Alq_3 (66nm)/Al. In terms of power efficiency, the device with a lower thickness of TPD (37 nm)/Alq_3 (66 nm) is the most efficient. It can be concluded that for high photometric efficiency and power efficiency, the devices ITO/TPD 1/Alq_3/Al must serve the following conditions, a) total organic layer thickness should be between 85 nm and 150 nm and b) thickness of Alq_3 layer should be larger than that of TPD 1 layer by about 10 to 20 nm.

This is in contrast to former published results of Tang et al.[3)], Forrest et al.[13,14)] according to which the thickness of HTL has no effect on efficiency. Moreover, Burrows et al. have reported that the current conduction and quantum efficiency in Alq_3 based OLEDs are controlled by electron trapping in the ETL. On the other hand, Antoniadis et al.[15,16)] and Riel et al.[18)] have emphasized the influence of the ITO/HTL interface on the operating voltage as well as the importance of HTL/ETL interface in determining the quantum efficiency for a two layer OLED. The results presented here are in agreement with the above conclusions of Antoniadis et al..

In order to investigate the influence of spiro-Qux on a TPD/Alq_3 device, the following experiment was carried out. Two different sectors, the first sector consisting of an Alq_3 layer thickness gradient (0-130 nm) and the second sector having two orthogonal gradients of Alq_3 and ETL (0-30 nm) were prepared on top of a TPD 1 layer with constant thickness (40 nm)[6)]. Aluminum (200 nm) was deposited through a mask with 49 holes. The active area of each

device is 0.19 cm^2 (spot with 2.54 mm radius). There is a linear gradient of 9.0 nm and 2.5 nm for Alq_3 and spiro-Qux layers in each device. Therefore the layer thicknesses were measured in the middle of each spot. Fig. 6a illustrates the two sectors created on the substrate.

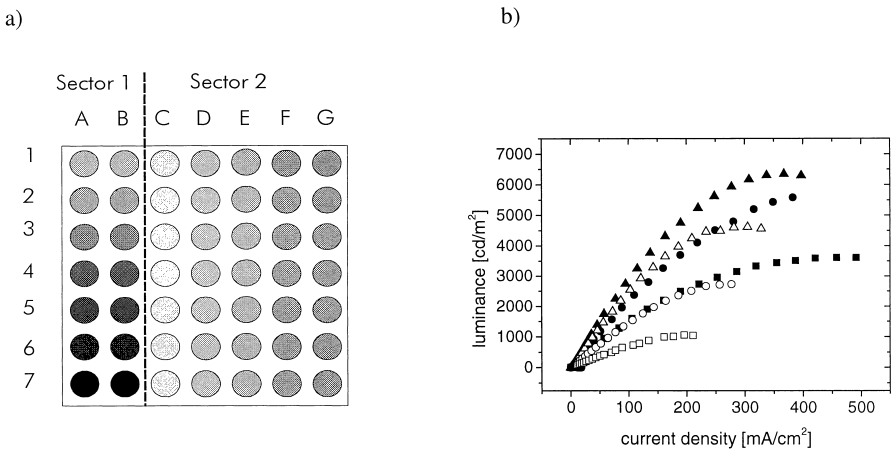

Figure 6: a) Schematic representation of a 7x7 OLED-matrix with an Alq_3 gradient (sector 1: rows A and B) and with an additional orthogonal gradient of ETL (sector 2: row C to G); b) luminance versus current density plot for the devices of row A (2-7) (Alq_3-thickness: ■ 31 nm; ● 49 nm; ▲67 nm; Δ 84 nm; ❍ 102 nm; □ 119 nm)

Sector 1 (1/3 area of substrate) has only an Alq_3-gradient and sector 2 (2/3 area of substrate) has orthogonal linear gradients of Alq_3 and spiro-Qux. With this device configuration, we were able to optimize the Alq_3-layer thickness for a constant TPD 1 layer thickness in sector 1 which is an internal reference for the three layer devices of ITO/TPD 1/Alq_3/ETL/Al in sector 2. The first sector (sector 1) allows to analyze the influence of the Alq_3 layer thickness variation with respect to the constant TPD 1 layer thickness of 40 nm. The luminance/current density characteristics of six of the devices (2A,3A,4A,5A,6A,7A) with the configuration ITO/TPD 1/Alq_3 (31 nm, 49 nm, 67 nm, 84 nm, 102 nm, 119 nm)/Al are plotted in fig. 6b. The device 4A with an Alq_3-layer thickness of 67 nm has the highest slope for luminance versus current density plot and reaches also the maximum luminance (about 6500 cd/m^2). The same device 4A also has the highest photometric efficiency. In sector 2 an additional spiro-Qux layer gradient was deposited orthogonal to the Alq_3-gradient. In fig. 7 the current-voltage-luminance characteristics of the device sequence 4C to 4G is compared with that of 4A without spiro-Qux. All these devices have the same Alq_3-layer thickness of 67 nm.

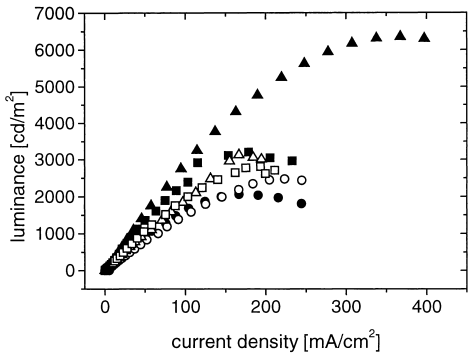

Figure 7: Comparison of luminance versus current density of device 4A (▲ without spiro-Qux) with devices 4C to 4G with a spiro-Qux thickness of: ■ 2 nm; ● 7 nm; ❍ 12 nm; Δ 17 nm and □ 21 nm.

There was no improvement found in the device characteristics by using an additional spiro-Qux layer. In order to examine other combinations of Alq_3 and spiro-Qux layer thicknesses, the photometric efficiency at 10 mA/cm^2 was plotted against the Alq_3 layer thickness and the spiro-Qux layer thickness in a three-dimensional graph (fig. 8). The behavior of photometric efficiency at 10 mA/cm^2 is observed for the whole current density range.

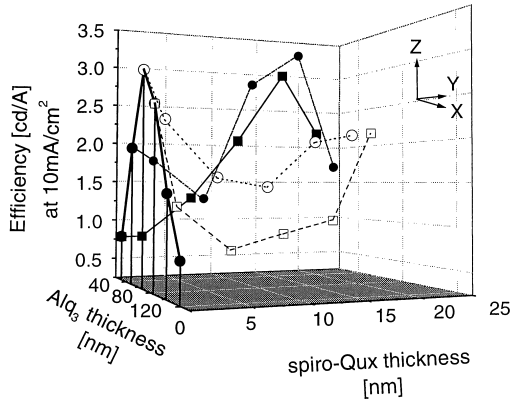

Figure 8: 3D-plot of photometric efficiency in cd/A against Alq_3- and spiro-Qux-layer thicknesses for selected devices without and with additional spiro-Qux: (■ row 2; ● row 3; ❍ row 4 and □ row 5).

The photometric efficiency of the devices with different Alq_3 layer thickness and without spiro-Qux as ETL (2A to 7A) is shown in the xz- plane. The photometric efficiency is plotted as a function of various ETL thicknesses and Alq_3 layer thicknesses in yz-plane. In row 2 (Alq_3-layer thickness: 31 nm) the photometric efficiency increases gradually with increasing thickness of spiro-Qux layer up to device 2F with an ETL layer thickness of 17 nm. On further increase in the thickness of ETL, the photometric efficiency decreases. On the other hand, for devices in rows 3, 4 and 5 with Alq_3 layer thicknesses of 49 nm, 67 nm and 84 nm respectively, the photometric efficiency first decreases and then increases with increasing spiro-Qux layer thickness. The device 2F, ITO/TPD (40 nm)/Alq_3 (31 nm)/spiro-Qux (17 nm)/Al shows higher photometric efficiency than the most efficient device 4A without an additional spiro-Qux layer. Similar to device 2F, the device 3F, ITO/TPD (40 nm)/Alq_3 (49 nm)/spiro-Qux (17 nm)/Al, also shows higher photometric efficiency than the device 4A. No improvement in efficiency was found for devices in rows 5 and 6 with 67 nm and 84 nm Alq_3 layer thicknesses using an additional spiro-Qux layer.

From the above results it can be concluded that the photometric efficiency of a device, ITO/TPD 1/Alq_3/Al with an Alq_3 layer thickness of 67 nm can be improved by about 10% using a combination of Alq_3 (31 nm)/spiro-Qux (17 nm) or Alq_3 (49 nm)/spiro-Qux (17 nm) layers.

The improvement in photometric efficiency caused by an additional spiro-Qux layer may be due to one or more of the following reasons: a) more effective electron injection, b) improved electron transport and c) better hole blocking effect of the spiro-Qux layer. In order to get a more detailed insight into the function of the spiro-Qux layer, the photometric efficiencies of the devices 4A, 2F and 3F were compared (fig. not shown). To obtain a photometric efficiency of about 2.5 to 3.0 cd/A in the high current region (>2 mA/cm^2), the current flow in 4A is considerably higher than that in 2F and 3F. This can be explained by a more efficient recombination of charges in 2F and 3F compared to that in 4A. This is a clear evidence for the hole blocking property of spiro-Qux. The efficiency in this kind of devices is determined by the effective injection and transport of minority charge carriers (electrons). Due to this fact, the variation of efficiency with respect to field can be correlated to the effectiveness of electron injection and/or transport. In order to obtain a photometric efficiency in the range of 1.0 to 3.0 cd/A, a considerably higher field has to be applied in devices 2F and 3F compared to that in device 4A. This fact indicates that the electron injection in device 4A with an Al/Alq_3-interface is better than in devices 2F and 3F with an Al/spiro-Qux-interface. A clear

picture about the electron transport capability of spiro-Qux could not be obtained from these experiments.

In row 4, there is no improvement in terms of power efficiency by using an additional spiro-Qux layer. For other thicknesses of Alq_3 layer, the power efficiency could be improved by an additional ETL in some cases. However, in all the tested three-layer devices, the power efficiency value of device 4A (ITO/TPD 1/Alq_3 (67 nm)/Al could not be reached. This is a result of the fact that higher fields are required for electron injection at an Al/spiro-Qux interface compared to Al/Alq_3 interface.

Conclusions

These results demonstrate that combinatorial method utilized in the device fabrication of OLEDs enables a rapid screening of materials under comparable conditions and a fast and efficient optimization of device configurations. Additional informations of device characteristics which are not detectable in conventional experiments can be elucidated out of these experiments. The considerable dependence of efficiency on Alq_3 layer thickness was observed for various TPD derivatives and the optimum thickness in each case was determined in a fast and efficient way. Moreover, the efficiency of a two layer TPD/Alq_3 device depends on both TPD and Alq_3 layer thicknesses. Further questions like the suitability and necessity of additional electron transport layers can also be addressed at using this method. The experiments with an additional spiro-Qux layer show an improvement in photometric efficiency for certain combinations of Alq_3/spiro-Qux layer thicknesses. The improvement in Alq_3/spiro-Qux devices can be attributed to the better hole blocking property of spiro-Qux. However, the power efficiency could not be improved by using an additional spiro-Qux layer due to the less efficient electron injection.

Acknowledgment

Financial support from SFB 481 „Complex macromolecular and hybrid systems in internal and external fields“ (projects A6 and B4) and Fonds der Chemischen Industrie - BMBF (C. Schmitz) is kindly acknowledged.

References

1. R. F. Service, *Science* **273**, 878 (1996).
2. J. Shi, C. W. Tang, *Appl. Phys. Lett* **70**, 1665 (1997).
3. C. W. Tang, S. A. VanSlyke, *Appl. Phys. Lett.* **51**, 913 (1987).
4. R. F. Service, *Science* **273**, 878 (1996).
5. Pioneer Electronic Corporation press release dated September 28, **1998**, (www.pioneer.co.jp/press/index-e.html).
6. C. Schmitz, P. Pösch, M. Thelakkat, H.-W. Schmidt, *Phys. Chem. Chem. Phys.* **1**, 1777 (1999)
7. C. Schmitz, M. Thelakkat, H.-W. Schmidt, *Adv. Mater.* **11**, 821 (1999).
8. J. J. Hanak, *J. Mater. Sci.* **5**, 964 (1970).
9. J. J. Hanak, V. Korsun, *Proceedings of the Fifteenth IEEE Photovoltaic Specialists Conference*, 780 (1978).
10. M. Thelakkat, H.-W. Schmidt, *Polym. Adv. Tech.* **9**(7), 429 (1998).
11. C. Adachi, K. Nagai and N. Tamoto, *Appl. Phys. Lett.* **66** (20), 2679 (1995).
12. M. Thelakkat, R. Fink, P. Pösch, J. Ring, H.-W. Schmidt, *Am. Chem. Soc.; Polym. Prep.* **38,** 394 (1997).
13. P. E. Burrows, S. R. Forrest, *Appl. Phys. Lett.* **64**(17), 2285 (1994).
14. P. E. Burrows, Z. Shen, V. Bulovic, D. M. McCarty, S. R. Forrest, *J. Appl. Phys.* **79**(10), 7991 (1996).
15. H. Antoniadis, J. N. Miller, D. B. Roitman, *IEEE Electron. Devices* **44**, 1289 (1997).
16. C. Giebeler, H. Antoniadis, D. D. C. Bradley, Y. Shirota, *J. Appl. Phys.* **85**(1), 608 (1999).
17. H. Riel, H. Vestweber, W. Riess, *Proc. SPIE* **240,** 3281 (1998).